Eur. Phys. J. B **6**, 519–528 (1998)

THE EUROPEAN PHYSICAL JOURNAL B

Tilt model of inverted amphiphilic mesophases

M. Hamm and M.M. Kozlov[a]

Department of Physiology and Pharmacology, Sackler Faculty of Medicine,
Tel-Aviv University, Tel Aviv 69978, Israel

Received: 9 February 1998 / Revised: 4 June 1998 / Accepted: 3 July 1998

Abstract. We present an alternative model of structure and energetics of the inverted amphiphilic mesophases. The previous studies of the inverted hexagonal, H_{II}, and inverted micellar cubic, Q_{II}, phases considered the amphiphilic monolayers to be homogeneously bent. In contrast, we assume a unit cell of an inverted mesophase to consist of flat fragments of monolayer. Hence, the unit cells of the H_{II} and Q_{II} phases are represented by a hexagonal rod and a polyhedron, respectively. Our model is motivated by Turner and Gruner's X-ray diffraction reconstruction of structure of the H_{II} phase. The only deformation of the amphiphilic monolayers we consider is tilt of the hydrocarbon chains with respect to the monolayer surface, determined by the packing constraints imposed in the mesophases. Applying our recent model for the elastic energy of tilt in liquid membranes [23], we show that: i) tilt accounts in a natural way for the frustration energy of mesophases resulting from filling by the hydrocarbon chains the corners of the unit cells, ii) the energy of tilt variation along the membrane surface is analogous to the bending energy. We compute the energetics of the H_{II}, Q_{IIsc} and Q_{IIfcc} phases and obtain a hypothetical phase diagram in terms of the elastic constants of monolayers. Moreover, we calculate the structural dimensions of the mesophases. We verify the model showing that the obtained phase diagram describes the recent data for the glycolipids/water systems; the predicted dimensions of the Q_{II} phase are in accord with the measured values; the model treats quantitatively the structural features observed for the H_{II} phase.

PACS. 68.10.-m Fluid surfaces and fluid-fluid interfaces – 68.10.Et Interface elasticity, viscosity, and viscoelasticity – 87.22.Bt Membrane and subcellular physics and structure

1 Introduction

Amphiphiles in water exhibit a variety of mesophases classified according to the shape of amphiphilic monolayers [1]. In the natural sequence of lyotropic liquid-crystalline phases, arranged according to their interfacial curvature [2] (Fig. 1), the lamellar L phase consisting of flat membranes (Fig. 1a) separates two classes of mesophases with curved monolayers. Conventionally, a mesophase is called normal (type I) if its monolayers are curved toward the hydrocarbon core, whereas the monolayers curved toward the aqueous solution form the inverted mesophases (type II). In geometrical terms, the amphiphilic monolayers of the normal and inverted mesophases are characterized by mean curvature [3] of opposite sign. The familiar examples are the cylindrical monolayers of the inverted, H_{II} (Fig. 1b), and normal, H_I (Fig. 1c), hexagonal phases and the spherical monolayers of the inverted, Q_{II} (Fig. 1d), and normal, Q_I (Fig. 1e), micellar cubic phases. Another class of mesophases, called the bicontinuous cubic phases, displays sponge like shapes of membranes, commonly described as periodic minimal surfaces of vanishing mean curvature [4]. A way to understand the mechanisms of phase behavior of amphiphiles is to consider the elastic energy of different mesophases [5].

In this work we will concentrate on the inverted phases of phospholipids, whose studies are motivated by attempts to understand the structural rearrangements of biological membranes resulting in their fusion [6–9], rupture, lateral phase separations and other important processes.

According to the common approach, there are two major factors determining the type of mesophase. The first is the spontaneous [10] or intrinsic [11] curvature, J_s, resulting from interplay of the attractive and repulsive interactions inside a monolayer [12]. Balance of these interactions leads to an effective curvature, J_s [13], determining an energetically preferable shape of the monolayer and, thus, the type of mesophase. A quantitative treatment of the effects of the spontaneous curvature is based on the bending model of amphiphilic monolayers [10].

The second factor results from the packing constraints imposed on the amphiphilic monolayers in the inverted and bicontinuous phases [8,14–19]. Besides the amphiphilic systems, the packing constraints have been shown to play an important role in phase behavior of block copolymers [20–22]. A simple illustration

[a] e-mail: misha@devil.tau.ac.il

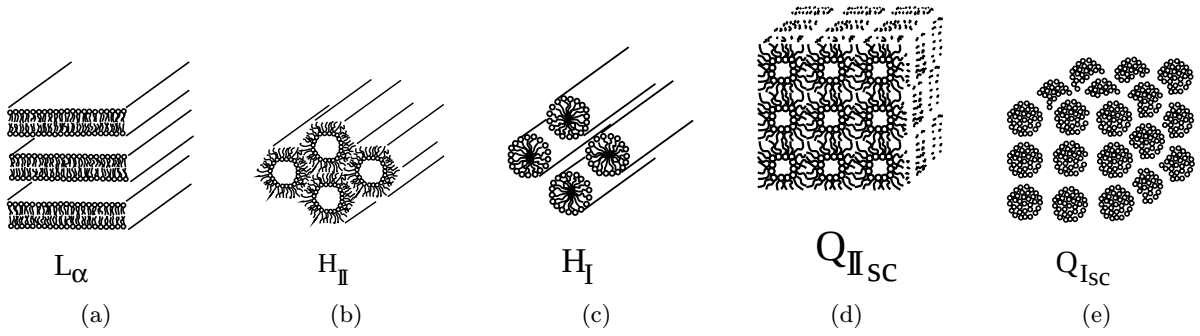

Fig. 1. Illustration of several amphiphilic mesophases: (a) Lamellar phase; (b) Inverted hexagonal H_{II} phase; (c) Normal hexagonal H_{II} phase; (d) Inverted micellar cubic Q_{II} phase; (e) Normal micellar cubic Q_I phase.

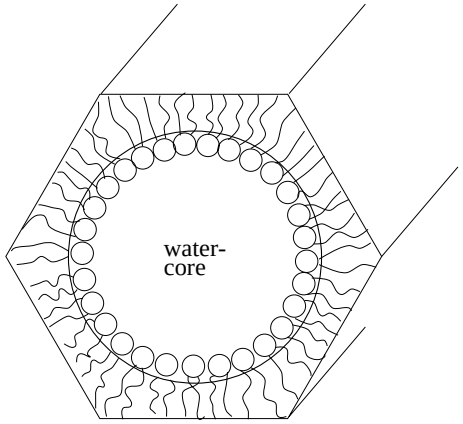

Fig. 2. Previously assumed [8,15–19] structure of a unit cell of the H_{II} phase with homogeneously curved interface between monolayer and water interior.

of this phenomenon is the inverted hexagonal H_{II} phase formed by identical long rods, each consisting of water core covered by lipid monolayer. The cross-sections of the rods represent unit cells of a two-dimensional hexagonal lattice (Fig. 1b). It was commonly assumed [8,15–19] that in a unit cell the hydrophilic interface between the monolayer and the water interior tends to adopt the shape of a circle with a curvature equal to the spontaneous curvature J_s (Fig. 2). On the other hand, according to the hexagonal symmetry of the lattice, the outer hydrophobic boundary of a unit cell is a hexagon (Fig. 2). Mismatch between the shapes of the hydrophilic and the hydrophobic boundaries of the monolayer leads to its additional deformations. The related energy is called the frustration energy [9]. Similar considerations illustrate the origin of the geometrical constraints and the frustration energy in the inverted micellar cubic phases, where the unit cells are packed in three-dimensional lattices. The reason for frustration of the bicontinuous cubic phases is related to the geometrical requirement of changing curvature along the monolayer surfaces [14].

Competition between the bending energy and the frustration energy has been assumed to drive the temperature-induced phase transition between the lamellar and the inverted hexagonal phase of phospholipid DOPE [8] and to determine a hypothetical phase diagram consisting in a sequence of the bicontinuous cubic, inverted hexagonal and inverted micellar cubic phases [17].

While the model for the bending energy is well established, the theoretical treatment of the frustration energy still poses a challenge since, on one hand, the exact character of deformations underlying the frustrations is unknown, and, on the other, the geometry of the packing constraints is, usually, too complicated to be taken into account by simple analytical means [17].

In the previous studies of lipid mesophases [14,17,18] the deformations of frustration have been treated solely in terms of stretch of the hydrocarbon chains filling the corners of the unit cells of mesophases so that the frustration energy results from the chain elasticity. Within the framework of these models it proved difficult to account systematically for the volume incompressibility of the hydrocarbon chains [17]. In addition, the elastic constant of the hydrocarbon chains determining the frustration energy, although estimated in a simple model [18], can not be directly compared with the experimental data and, thus, remains an adjusting parameter. As a results of these and other complications mentioned in [17], the model of chain stretching, although describing qualitatively the expected phase diagrams, has difficulties with correct predictions of the linear dimensions of the cubic phases resulting from the phase transitions [17] and with reproducing the previously estimated value of the frustration energy [18].

The present study is devoted to an alternative model for the frustration energy of the inverted mesophases based on assumption that the major deformation induced by the packing constraints is tilt of the hydrocarbon chain with respect to the membrane surface [23]. The main motivation of our work is due to the Turner and Gruner's reconstruction of the inverted hexagonal H_{II} phase in lipid-water systems [24]. According to these data, the hydrophilic boundary of a monolayer in a unit cell of the H_{II} phase tends to mimic the hexagonal shape of the outer boundary. The observed shape of the hy-

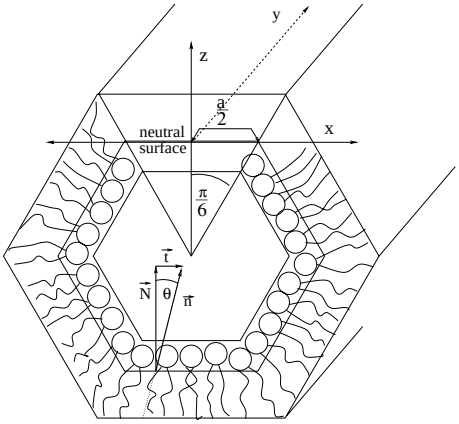

Fig. 3. Structure of a unit cell of the H_{II} phase considered in the present work. In contrast to the previous model (Fig. 2), the unit cell consists of six identical *flat* fragments of monolayer called cassettes.

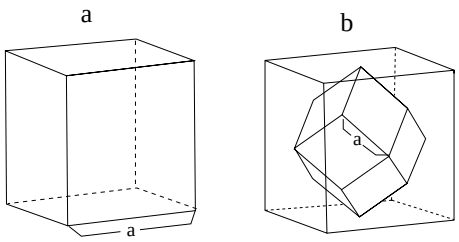

Fig. 4. Unit cells of the inverted micellar cubic phases; (a) *sc* phase; (b) *fcc* cell. Only the dividing surface of monolayer forming a unit cell is shown.

drophilic boundary is reminiscent of a hexagon with rounded corners, rather than a circle [24]. Similar shape has been recently obtained theoretically by self-consistent field approach for interface between domains of different blocks in cylindrical phase of diblock copolymers [20].

To study the consequences of this observation for the energetics of the mesophases we adopt a model different from those analyzed previously. We assume that the hydrophilic surface imitates exactly the shape of the outer boundary of the unit cell, *i.e.* is a hexagon for the H_{II} (Fig. 3) phase and a polyhedron for Q_{II} phase (Fig. 4). Thus, the fragments of monolayer, constituting a unit cell, remain flat, but the amphiphilic molecules are tilted with respect to the monolayer surface. Moreover, the tilt considerably changes along the monolayer, reaching its maximal value in the corners of the unit cell. In this representation, the energy of a mesophase is determined solely by the tilt and its variation.

Using our recent consideration of the tilt energy of fluid membranes [23], we analyze the energetics of different inverted mesophases and show that the suggested approach not just qualitatively describes the sequences of the lamellar, inverted hexagonal and inverted cubic phases registered in glycolipid/water systems [2], but also predicts a correct order of magnitude of structural dimensions of the cubic phases [25] and explains the structural features of the H_{II} [26].

However, it is necessary to emphasize that the suggested model is not exact as it neglects the fact that the corners of elementary cells of the inverted hexagonal and cubic phases are rounded, as observed for the H_{II} phase of phospholipid [24]. According to the experimental results [24], the characteristic length of such rounding is small compared to dimension of an elementary cell, what justifies the assumptions of our model. Nevertheless, consideration of energetics of rounded corners going beyond the goal of the present study, is the matter of further sophistication of the model.

2 Model

We consider an amphiphilic monolayer in liquid state, whose hydrocarbon core has properties of an incompressible elastic continuum [23]. To describe the geometry and the deformations of the monolayer we use the dividing surface [27] lying along the interface between the polar groups and the hydrocarbon interior [19,28] and shown for the particular lipids to play a role of a neutral surface [28]. The shape of the monolayer will be identified with the shape of its dividing surface.

We assume the monolayers to form the lamellar L phase, the inverted hexagonal H_{II} phase and two inverted micellar cubic Q_{II} phases with different symmetries. Each mesophase is a periodic structure consisting of equivalent unit cells, which are obtained by the Wigner-Seitz construction.

In the lamellar phase the monolayers are flat (Fig. 1a). In a unit cell of the H_{II} phase the monolayer is an infinite cylinder with hexagonal cross-section (Fig. 3). The monolayers of unit cells of the Q_{II} phases are polyhedra (Fig. 4) corresponding to *sc* (Fig. 4a) and *fcc* (Fig. 4b) lattice structures. The mesophases are fully hydrated and can exchange water with the surrounding medium, thus, changing the sizes of their unit cells, if it results in minimization of the energy.

It is important to underline again that in our model, the dividing surfaces of monolayers in units cells of the H_{II} and Q_{II} phases consist of flat fragments, characterized by vanishing curvature. Moreover, we assume that the area per amphiphilic molecule at the dividing surface is constant and equal in all the mesophases. Thus, the monolayers in the mesophases are not bent and their molecular area is not changed. Instead of that, they are subject to deformation of tilt of the hydrocarbon chains with respect to the dividing surface. The tilt is determined by requirement that no vacuum is allowed in the system, so that the space between the dividing surface and the outer boundary of a unit cell must be filled by the hydrocarbon chains. The illustration of this constraint resulting in tilt of the hydrocarbon chains in presented in (Fig. 3) for the H_{II} phase, while for the cubic phases it is analogous although more complicated to illustrate graphically.

We quantify the tilt $\mathbf{t}$ by deviation of a unit vector $\mathbf{n}$ indicating the average direction of the hydrocarbon

chains from the unit normal to the dividing surface $\mathbf{N}$ (Fig. 3) [23]

$$\mathbf{t} = \frac{\mathbf{n}}{\mathbf{nN}} - \mathbf{N}. \tag{1}$$

The tilt vectors is parallel to the dividing surface, $\mathbf{t}\cdot\mathbf{N} = 0$, and its absolute value is the tangent of the angle θ between the vectors $\mathbf{n}$ and $\mathbf{N}$.

The elastic energy f of tilt is determined, on one hand, by the tilt vector, $\mathbf{t}$, itself and, on the other, by its change along the dividing surface. To quantify the latter we choose a rectangular system of coordinates $\{x, y\}$ related to a flat fragment of the dividing surface (Fig. 3) and denote the derivatives of $\mathbf{t}$ in the directions of the axis by $\mathbf{t}_\xi = \frac{\partial \mathbf{t}}{\partial \xi}$, with $\xi = x, y$. The components of the two vectors, $\mathbf{t}_x$, $\mathbf{t}_y$ form a tensor called the tilt tensor $t^\xi{}_\zeta$, the Greek indices indicating the surface coordinates x, y [23]. The elastic energy per unit area of the dividing surface can be written as [29,23]

$$f = \frac{1}{2}\kappa(t^\xi{}_\xi + J_s)^2 + \bar{\kappa}\det(t^\xi{}_\zeta) + \frac{1}{2}\kappa_\theta \mathbf{t}^2 \tag{2}$$

where $\det(t^\xi{}_\zeta)$ and $t^\xi{}_\xi$ are, respectively, the determinant and the trace of the tilt tensor, the latter equal to the two-dimensional divergence of the tilt vector, $t^\xi{}_\xi = \mathrm{div}(\mathbf{t})$. The values κ and $\bar{\kappa}$ are the bending modulus and the modulus of Gaussian curvature of the monolayer, respectively, J_s is the spontaneous curvature of the monolayer, and κ_θ is the monolayer tilt modulus.

A detailed derivation of the Hamiltonian (2) accounting for contributions up to the second order in the deformations $\mathbf{t}$ and $t^\xi{}_\zeta$ is presented elsewhere [23]. However, the form (2) of the Hamiltonian can be directly understood on the basis of two classical works by Frank [29] and Helfrich [10]. Comparing the definitions above (see also [23]) with those of [29], one see that the tilt tensor $t^\xi{}_\zeta$ accounts for the deformations of splay and twist introduced by Frank for liquid crystals [29]. Specifically, the diagonal components of $t^\xi{}_\zeta$ represent the components of splay, denoted in [29] as s_1, s_2, while the nondiagonal components of $t^\xi{}_\zeta$ are analogous (up to an arbitrary choice of sign) to the components of twist τ_1, τ_2 [29]. The trace $t^\xi{}_\xi$ and the determinant $\det(t^\xi{}_\zeta)$ of the tilt tensor are equivalent, respectively, to the total splay, $s_1 + s_2$, and the saddle splay, $s_1\, s_2 + \tau_1\, \tau_2$, as defined by Frank [29]. Hence, the first and second terms in (2) represent the Frank energy of total splay and that of saddle splay. As emphasized by Helfrich [10], the total and saddle splay in the case of a membrane are analogous to the total and Gaussian curvature, respectively. As a result, the elastic coefficients determining the related contributions to the energy (2) are equal to the bending modulus κ and the modulus of Gaussian curvature $\bar{\kappa}$ [10], while the "optimum degree of splay" s_0 [29] is equivalent to the Helfrich spontaneous curvature J_s.

The third contribution to the energy (2) is appropriate only for tilt and is determined by an independent elastic constant κ_θ [10].

An explicit consideration of a combined deformation of a fluid membrane determined by tilt tensor, tilt *per se* and bending including computation of the relevant elastic constants is performed in [23]. The Hamiltonian (2) results from the equation of [23] in a case of vanishing bending.

The bending rigidity κ and the tilt modulus κ_θ are directly related to the elastic moduli of the monolayer interior [23] and have to be positive to provide the mechanical stability of the system, $\kappa, \kappa_\theta > 0$. On the other hand, the spontaneous curvature J_s and the modulus of Gaussian curvature $\bar{\kappa}$ are expressed through the distribution of the microscopic stresses over the monolayer thickness [23], their sign depending on the monolayer structure.

The possible behavior of the tilt tensor $t^\xi{}_\zeta$ is limited by the geometrical constraints of our model, specifically, by i) the condition that the dividing surfaces are flat and parallel to the outer boundaries of the unit cells; ii) the incompressibility of the monolayer material; iii) the constancy of molecular area at the dividing surface. The local distance z between the dividing surface and the outer boundary of the unit cell (Fig. 3) can be expressed [23] within the accuracy of our model as

$$z = z_0(1 - \frac{1}{2} z_0\, t^\xi{}_\xi) \tag{3}$$

where z_0 is the value of z in undeformed state. For parallel surfaces the distance z does not change, what means that the trace of the tilt tensor $t^\xi{}_\xi$ has to remain constant along the dividing surface, $t^\xi{}_\xi = const.$

Based on the elastic model (2), we calculate the average energy per unit area of the dividing surface in all the considered mesophases as functions of the elastic parameters. Comparing these energies we will construct the phase diagram.

3 Energetics of mesophases and phase diagram

3.1 Lamellar phase

In the lamellar L phase all the amphiphilic molecules are subject to the same packing constraints and the properties of the monolayers are assumed to be isotropic and homogeneous along the flat dividing surface of the amphiphilic film. Therefore, the tilt vanishes everywhere, $\mathbf{t} = 0, t^\xi{}_\zeta = 0$ and the average elastic energy (2) is

$$\langle f_L \rangle = \frac{1}{2}\kappa J_s^2. \tag{4}$$

3.2 Inverted hexagonal H_{II} phase

The monolayer of a hexagonal rod representing a unit cell of the H_{II} consists of six equal cassettes. Thus we consider one cassette (Fig. 3) and choose the $\{x, y\}$ system of coordinates in the plane of the dividing surface, so that

the y-axis is directed along the axis of the rod, and the x-axis is perpendicular to it with the origin ($x = 0$) in the middle of the cassette cross-section (Fig. 3).

The hexagonal rod is seen as infinitely long compared to its cross-section. Thus, for the reasons of symmetry we assume that the properties of the monolayers are homogeneous along the rod axis and the corresponding y-component of the tilt vector vanishes

$$t_y = 0. \tag{5}$$

On the other hand, the tilt of the hydrocarbon chains in the x-direction, t_x, has to develop in order to fill the corners of the unit cell of the hexagonal lattice (Fig. 3).

In the middle of the cassette, $x = 0$, tilt vanishes for the reasons of symmetry, while at its boundaries the angle θ between the vectors $\mathbf{n}$ and $\mathbf{N}$ adopts the values $\pm\frac{\pi}{6}$ so that the absolute value of the tilt vector becomes $\pm\frac{1}{\sqrt{3}}$. Accounting for these conditions together with the requirement (3) we obtain

$$t_x(x) = \frac{2}{\sqrt{3}}\frac{x}{a} \tag{6}$$

where a is the length of the unit cell side determined at the dividing surface (Fig. 3).

According to (5, 6) the tilt tensor has only one non-vanishing component

$$t^x{}_x = \frac{\partial t_x}{\partial x} = \frac{2}{\sqrt{3}}\frac{1}{a}\,. \tag{7}$$

Hence, its determinant vanishes, $\det(t^\xi{}_\xi) = 0$, what is analogous to the vanishing Gaussian curvature of cylindrical surfaces.

Inserting (5–7) in (2) we obtain the energy per unit area as a function of the position x along the dividing surface

$$f_{H_{II}} = \frac{1}{2}\kappa\left(\frac{2}{\sqrt{3}a} + J_s\right)^2 + \frac{2}{3}\kappa_\theta\left(\frac{x}{a}\right)^2.$$

Averaging this energy over the area of the cassette, we obtain

$$\langle f_{H_{II}}\rangle = \frac{1}{2}\kappa\left(\frac{2}{\sqrt{3}a} + J_s\right)^2 + \frac{\kappa_\theta}{18}\,. \tag{8}$$

Remarkable feature of (8) is that its first term, analogous to the bending energy, depends on the linear dimension a of a unit cell, while the second, related to the tilt modulus κ_θ, is independent from a.

The linear dimension a minimizing the bending energy contribution to (8) is,

$$a^*_{H_{II}} = -\frac{2}{\sqrt{3}}\frac{1}{J_s}\,. \tag{9}$$

The negative sign in the right side of (9) means that the energy (8) can be minimized if the spontaneous curvature J_s is negative. According to the convention adopted in [23] and in the present work, the negative sign of J_s indicates a tendency of the monolayer to bend spontaneously towards the water volume or to display due to the tilt the corresponding splay of the hydrocarbon chains.

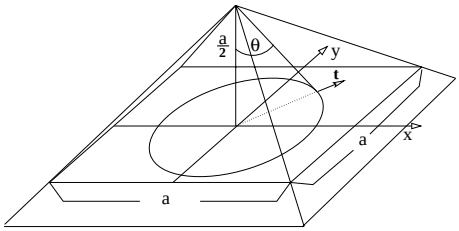

Fig. 5. One cassette of a unit cell of *sc* phase.

We will assume everywhere below the spontaneous curvature of a monolayer to be negative, $J_s < 0$.

The final average energy of the H_{II} phase,

$$\langle f^*_{H_{II}}\rangle = \frac{\kappa_\theta}{18}, \tag{10}$$

is determined solely by the tilt modulus κ_θ. This energy can not be influenced by changing the linear dimension of a unit cell and is, obviously, related to the lattice structure. Hence, the contribution to the energy proportional to κ_θ is the most direct characteristics of the packing constraints of the lattice and will be called the frustration energy.

3.3 Inverted micellar cubic Q_{II} phases

Calculation of the energies of the cubic phases, although more complicated, proceeds analogously to that of the H_{II} phase. We will sketch the calculation for the simple cubic Q_{IIsc} phase and present the results obtained for the Q_{IIfcc} phase.

A unit cell of the Q_{IIsc} is a cube consisting of 6 equal square cassettes (Fig. 4a). Hence, we consider one of them illustrated in Figure 5. The system of coordinates has its origin in the middle of the dividing surface of the cassette and is oriented as shown in (Fig. 5). The tilt vector has two non- vanishing components, $\mathbf{t} = \{t_x, t_y\}$. They can be determined from the condition (3) and the boundary conditions imposed on the change of the angle θ (between the vectors $\mathbf{n}$ and $\mathbf{N}$) along the circumference of the square. Accounting for the symmetry of the simple cubic unit cell we obtain

$$t_x = \frac{2}{a}x, \quad t_y = \frac{2}{a}y \tag{11}$$

where a is the length of the square side at the dividing surface (Fig. 5), characterizing, as above, the linear dimension of the unit cell. The two diagonal components of the tilt tensor do not vanish in this case, $t^x{}_x = t^y{}_y = \frac{2}{a}$. Thus, both the trace and determinant of the tilt tensor $t^\xi{}_\zeta$ together with the tilt vector (1) contribute to the elastic energy (2). Averaging this energy over the area of the

cassette we obtain

$$\langle f_{Q_{IIsc}} \rangle = \frac{1}{2}\kappa\left(\frac{4}{a} + J_s\right)^2 + \bar{\kappa}\frac{4}{a^2} + \frac{\kappa_\theta}{3}\,. \qquad (12)$$

Minimization of the energy (12) with respect to the linear dimension a results in

$$\langle f^*_{Q_{IIsc}} \rangle = \frac{1}{2}\frac{\kappa\,\bar{\kappa}}{2\kappa + \bar{\kappa}}J_s^2 + \frac{\kappa_\theta}{3}\,. \qquad (13)$$

In contrast to (10), the energy (13) contains the contribution determined by the elastic moduli κ, $\bar{\kappa}$ and the spontaneous curvature J_s. This is expected as the unit cell of Q_{II} phase is analogous to a closed monolayer of spherical topology, characterized by non-vanishing energy contribution of the Gaussian curvature. This contribution results in competition of two tendencies. The first is minimization of the energy proportional to the bending rigidity κ and leading to $a \to -4/J_s$. The second is related to the term proportional to the modulus of Gaussian curvature and consists in increase or decrease of the linear dimension a depending on sign of $\bar{\kappa}$.

The resulting equilibrium linear dimension of the unit cell is

$$a^*_{Q_{IIsc}} = -2\left(2 + \frac{\bar{\kappa}}{\kappa}\right)\frac{1}{J_s}\,. \qquad (14)$$

Since the spontaneous curvature J_s is assumed to be negative, the expression (14) implies

$$\left(2 + \frac{\bar{\kappa}}{\kappa}\right) > 0. \qquad (15)$$

We will assume everywhere below the condition (15), which is the familiar criterion of stability of membranes with respect to vesiculation [31], to be satisfied.

Performing an analogous calculation for the cubic phase with fcc-lattice we take into account that a unit cell consists of 12 equal rhombic cassettes (Fig. 4b). Consideration of symmetry of a unit cell together with the condition (3) results in distribution of components of the tilt vector along the dividing surface of one cassette , $t_x = \frac{2}{\sqrt{3}}\frac{x}{a}$ $t_y = \frac{2}{\sqrt{3}}\frac{y}{a}$. Based on this expressions we obtain the average energy

$$\langle f^*_{Q_{IIfcc}} \rangle = \frac{1}{2}\frac{\kappa\,\bar{\kappa}}{2\kappa + \bar{\kappa}}J_s^2 + \frac{\kappa_\theta}{9} \qquad (16)$$

and the linear dimension of a unit cell

$$a^*_{Q_{IIfcc}} = -\frac{2}{\sqrt{3}}\left(2 + \frac{\bar{\kappa}}{\kappa}\right)\frac{1}{J_s}.$$

The values of the frustration energy of the two cubic phases represented by the last terms in (13, 16) are larger than that of the H_{II} phase (10). This is expected, as the packing constraints are recognized to be stronger in the inverted cubic Q_{II} phases than in the H_{II} phase [17].

Table 1. Energy per unit area and linear dimension of elementary cell of different phases.

phase	energy per area $\langle f^* \rangle$	a^*
L_α	$\frac{1}{2}\kappa J_s^2$	
H_{II}	$\frac{\kappa_\theta}{18}$	$\frac{2}{\sqrt{3}(-J_s)}$
$Q_{II\,sc}$	$\frac{1}{3}\kappa_\theta + \frac{1}{2}\frac{\bar{\kappa}}{2\kappa+\bar{\kappa}}\kappa J_s^2$	$\frac{2}{(-J_s)}(2 + \frac{\bar{\kappa}}{\kappa})$
$Q_{II\,fcc}$	$\frac{1}{9}\kappa_\theta + \frac{1}{2}\frac{\bar{\kappa}}{2\kappa+\bar{\kappa}}\kappa J_s^2$	$\frac{2}{\sqrt{3}(-J_s)}(2 + \frac{\bar{\kappa}}{\kappa})$

The results obtained for the different mesophases are summarized in Table 1.

3.4 Phase diagram

A mesophase with minimal energy is the stable one. Comparing the energies of different mesophases (Tab. 1) we construct a hypothetical phase diagram as a function of the elastic parameters of amphiphilic monolayer κ, $\bar{\kappa}$, κ_θ and J_s.

The structure of the expressions for the energies (Tab. 1) makes it convenient to scale the elastic moduli in units of the bending modulus κ. We thus define a dimensionless parameter $\xi = \frac{\bar{\kappa}}{\kappa}$ and a characteristic length, $\lambda = \sqrt{\frac{\kappa}{\kappa_\theta}}$. The phase diagram will be determined by the dimensionless order parameters ξ and λJ_s.

Consider first the two cubic phases, Q_{IIsc} and Q_{IIfcc}, whose unit cells have a similar spherical topology, but different symmetry. The contributions analogous to the bending energy and determined by the elastic parameters κ, $\bar{\kappa}$ and J_s are equal for the two phases. This is related to the similarity of topology [32]. In contrast, due to the different symmetries the frustration energy is smaller in the Q_{IIfcc} phase. The number of cassettes in a Q_{IIfcc} unit cell is larger than in a simple cubic one, Q_{IIsc}. Thus, the maximal tilt angle, which has to be reached at the boundary of the cassette is smaller and, hence, the geometrical constraints are weaker in the Q_{IIfcc} than in the Q_{IIsc} phase. As a result, the simple cubic, Q_{IIsc} phase is energetically less favorable than the Q_{IIfcc} phase for all feasible values of the elastic parameters [33]. Similar results have been obtained in a general form for colloidal crystals [34–36]. We will not further consider the Q_{IIsc} phase referring for simplicity to Q_{IIfcc} as to Q_{II} phase.

Now we compare the energies of inverted hexagonal H_{II} phase, $\langle f^*_{H_{II}} \rangle$, and that of the inverted cubic Q_{II} phase, $\langle f^*_{Q_{II}} \rangle$. The frustration energy of the H_{II} phase is two times smaller than that of the Q_{II} phase (Tab. 1). On the other hand, $\langle f^*_{Q_{II}} \rangle$, in contrast to $\langle f^*_{H_{II}} \rangle$, has a contribution analogous to the bending energy. The sign of this contribution is determined by the modulus of Gaussian curvature $\bar{\kappa}$.

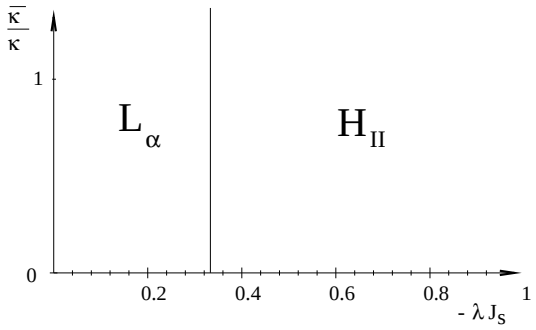

Fig. 6. Phase diagram at positive modulus of Gaussian curvature, $\bar{\kappa} > 0$.

Table 2. Equations of phase boundaries between different pairs of phases.

L_α-H_{II}	$\frac{1}{3}$	=	$(-\lambda J_s)$
L_α-$Q_{II\,fcc}$	$(-\bar{\kappa}/\kappa)$	=	$2 - 9(-\lambda J_s)^2$
H_{II}-$Q_{II\,fcc}$	$(-\bar{\kappa}/\kappa)$	=	$\frac{2}{1+9(-\lambda J_s)^2}$

If $\bar{\kappa} > 0$, the bending contribution further increases the energy $\langle f^*_{Q_{II}} \rangle$ with respect to $\langle f^*_{H_{II}} \rangle$ so that the Q_{II} phase remains energetically less favorable than the H_{II} phase for all values of the other parameters. The phase diagram involves in this case only the lamellar and the inverted hexagonal phases (Fig. 6) and is determined solely by the variable λJ_s. Transition from the lamellar to the inverted hexagonal, H_{II}, phase occurs at $\lambda J_s = -\frac{1}{3}$.

If the modulus of Gaussian curvature is negative, $\bar{\kappa} < 0$, the energy $\langle f^*_{Q_{II}} \rangle$ can become smaller than $\langle f^*_{H_{II}} \rangle$, and the inverted micellar cubic Q_{II} phase comes into play. The resulting phase diagram involving all three phases is presented in Figure 7. The equations for the curves of coexistence of pairs of phases determining the phase boundaries in Figure 7 are summarized in Table 2. The phase diagram consists of three regions separated by the solid lines. The cubic phase occupies the upper part of the phase diagram corresponding to the most negative values of the modulus of the Gaussian curvature $\bar{\kappa}$. The bottom part of the phase diagram is shared by the lamellar, L, and the inverted hexagonal, H_{II}, phases, the latter occupying the range of the more negative values of the spontaneous curvature J_s. The point of coexistence of all three phases (the triple point) corresponds to the values of the order parameters, $\sqrt{\frac{\kappa}{\kappa_\theta}} J_s = -1$, $\frac{\bar{\kappa}}{\kappa} = -\frac{1}{3}$. According to the phase diagram (Fig. 7), a hypothetical experiment consisting in a gradual change of the spontaneous curvature, J_s, of monolayer at fixed values of the other elastic parameters, can result in a direct transition from the lamellar to the cubic phase, L-Q_{II}, or in a sequence of phases including the hexagonal phase, L-H_{II}-Q_{II}, depending on the value of the modulus of Gaussian curvature $\bar{\kappa}$.

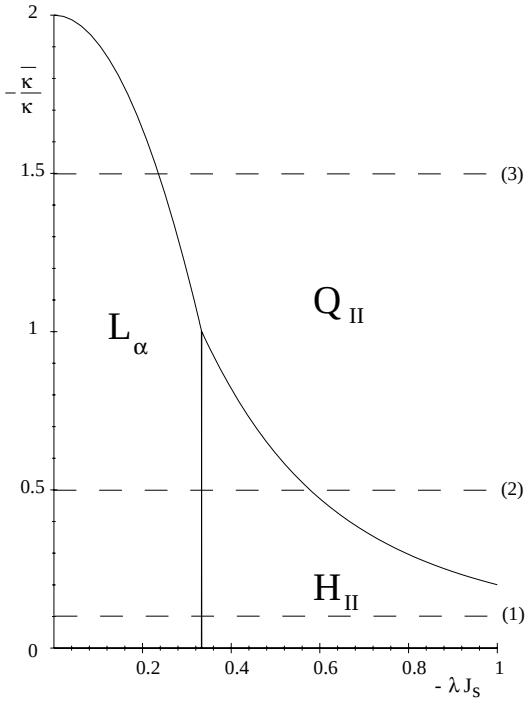

Fig. 7. Phase diagram at negative modulus of Gaussian curvature $\bar{\kappa} < 0$. Solid lines determine the phase boundaries. The dashed lines (1), (2) and (3) indicate hypothetical trajectories of the system along the phase diagram at different values of $\bar{\kappa}$.

For comparison of the model with experimental results it is instructive to derive the characteristic dimensions of the phases in the points of phase transition. We will relate to the linear dimension of a unit cell a presented in Table 1. Based on this value and accounting for the dimension of the polar heads of amphiphilic molecules, one can easily calculate for each mesophase the dimension of the water core of a unit cell, or, taking into account the volume of the hydrocarbon chains, one can compute the dimension of the outer boundary of a unit cell and the repeating distances of the lattice. Inserting the conditions of phase transitions expressed by the coexistence curves (Tab. 2) into the equations for a of the H_{II} and Q_{II} phases (Tab. 1) we obtain the linear dimensions a^* at phase transitions summarized in Table 3. The values of a^* scale with the characteristic length λ. For the transition between the L and H_{II} phases, the dimensionless value $\frac{a^*}{\lambda}$ is a fixed number, $2\sqrt{3}$, while for the other phase transitions it depends on the dimensionless spontaneous curvature λJ_s, as illustrated in Figure 8. A remarkable feature of the linear dimension a^* is that in the triple point it is equal $\frac{a^*}{\lambda} = 2\sqrt{3}$ both for the H_{II} and Q_{II} phases. This is not determined by general thermodynamic requirement and holds only for the specific cubic phase with *fcc* symmetry we consider.

Table 3. Linear dimension of elementary cell of different phases at phase boundaries.

coexistence curve	phase	a^*/λ
L_α-H_{II}	H_{II}	$2\sqrt{3}$
L_α-$Q_{II\,fcc}$	$Q_{II\,fcc}$	$6\sqrt{3}(-\lambda J_s)$
H_{II}-$Q_{II\,fcc}$	H_{II}	$\frac{2}{\sqrt{3}}\frac{1}{(-\lambda J_s)}$
H_{II}-$Q_{II\,fcc}$	$Q_{II\,fcc}$	$\frac{4}{\sqrt{3}}\frac{1}{(-\lambda J_s)}\left(1-\frac{1}{1+9(\lambda J_s)^2}\right)$

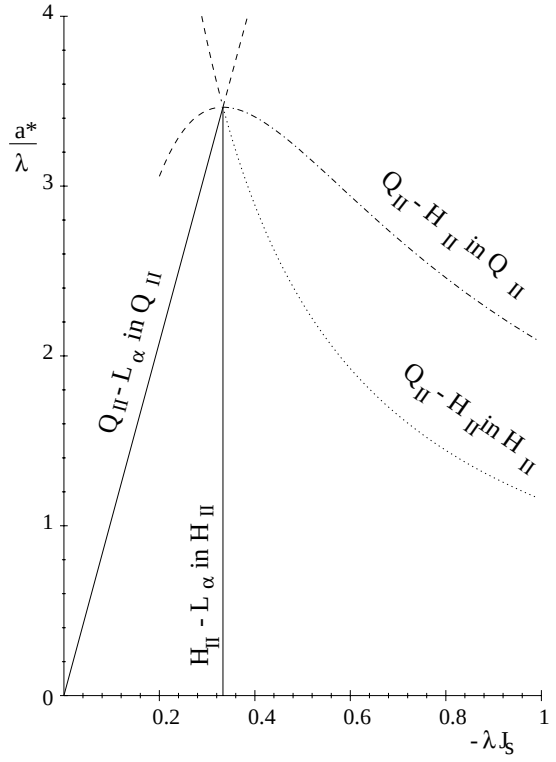

Fig. 8. Diagram of linear dimensions of the mesophases at phase transitions.

4 Discussion

We presented an alternative model of energetics and structure of the inverted amphiphilic mesophases.

The approach suggested in the present study addresses in a natural way the packing constraints in the inverted mesophases. The corners of the unit cells are filled by the hydrophobic material due to the tilt of the hydrocarbon chains linearly changing along the monolayer surface. The volume incompressibility of the hydrocarbon material is accurately taken into account by the change of the distance between the monolayer dividing surface and the outer boundary of the unit cell, as determined by equation (3).

The frustration energy in our model is equal to the tilt modulus κ_θ multiplied by a coefficient depending on the type of mesophase. While this coefficient can be calculated for each mesophase (Tab. 1), the tilt modulus κ_θ is independent from all measured elastic constants of amphiphilic monolayers and remains to be determined experimentally. However, we can estimate κ_θ. The value of the frustration energy per lipid (DOPE) molecule in the H_{II} phase, obtained according to Siegel's approach [8] is $0.352kT$ [19] (where k is the Boltzmann constant and T is the absolute temperature). On the other hand, according to our model (Tab. 1) this energy equals $\frac{1}{18}\kappa_\theta s$, where s is the area per molecule at the dividing surface $s = 0.65\,\mathrm{nm}^2$ [26]. Thus, we obtain for the tilt modulus

$$\kappa_\theta = 40\frac{mJ}{m^2}\cdot \tag{17}$$

This value is in accord with the crude estimation performed in [23] using a oversimplified molecular model. Let us emphasize that the value (18) is determined for particular phospholipid DOPE. The suggested model does not allow for any generalization of this result such as determination of the chain length dependence of the tilt modulus κ_θ.

Using the available values of the bending rigidity, $\kappa \simeq 4.2\times10^{-20}J$, and the spontaneous curvature, $J_s \simeq \frac{1}{3}\,\mathrm{nm}^{-1}$, of DOPE monolayer [19], and the estimated value of the tilt modulus κ_θ (18), we can verify the model.

All the inverted cubic phases recently registered experimentally [2,25] have the *Fd3m* symmetry, what is different from the *fcc* cubic phase we considered in this work. The accurate calculations for the *Fd3m* phase can be done in our model, but turns out to be very complicated because of the complex geometry of unit cells. On the other hand, we performed the calculations (not shown) for the *bcc* cubic phase approaching in its complexity the *Fd3m* phase, and obtained the energy, $\langle f^*\rangle$, and the linear dimension of a unit cell, a^*, close to those of the *fcc* phase [37]. Therefore, we treat approximately the experimental results on the *Fd3m* [2,25] by the model predictions received for the *fcc* phase.

In homologous series of dialkyl α- and β-D-xylopyranosylglycerols one observed three different sequences of temperature-induced phase transitions, the character of the sequence depending on the hydrocarbon chain length. For the short chains the sequence was L-to-H_{II}, for the intermediate chain length one found the sequence L-to-H_{II}-to-Q_{II} and, finally, for the longest chains the L-to-Q_{II} transition has been registered [2].

All these sequences of phases are predicted by the phase diagram (Fig. 7) if one assume, according to [38], that the modulus of Gaussian curvature $\bar{\kappa}$ becomes more negative with the chain length, and increase in the temperature drives the spontaneous curvature J_s to the more negative values [19]. Hence, for the short chains the trajectory of the system along the phase diagram is expected to lie in its bottom part and to cross only the boundary between the L and H_{II} phases (Fig. 7, (1)), for the intermediate chain length, the trajectory crosses two boundaries, L-H_{II} and H_{II}-Q_{II} (Fig. 7, (2)), and, finally for the

longest chain length, the trajectory intersects only the L-Q_{II} boundary (Fig. 7, (3)). Although our theory suits the cited experimental observation, it should be noted, that in the case of the xylolipids the lamellar L phase does not expose lateral fluidity.

The measurements [25] provided one with an estimation of the dimension of the water core of the $Fd\bar{3}m$ cubic phase of the order of 1 nm. In our model, according to the above values of the elastic parameters, the characteristic length determining the linear dimensions of the unit cells of mesophases at phase transition is $\sqrt{\frac{\kappa}{\kappa_\theta}} \simeq 1\,\mathrm{nm}$. Thus, the linear dimension of the cubic phase a^* is of the order of $2-3\,\mathrm{nm}$ (Fig. 8). To estimate the dimension of the water core we account for the thickness of the layer of polar heads separating the dividing surface, from the water interior and obtain $1-2\,\mathrm{nm}$, what agrees in the order of magnitude with the experimental results [25].

The linear dimensions of unit cells of the H_{II} phases resulting from X-rays data have been accurately calculated for DOPE in the point of phase transition between the lamellar and the inverted hexagonal phases [26]. It has been shown that the thickness z of the monolayer in the middle of a cassette of the H_{II} phase unit cell is 25% smaller than the thickness z_0 of a monolayer in the L phase. To treat this observation the authors [26] assumed that the hydrocarbon chains are tilted along the cylinder axis resulting in breaking the symmetry in this direction. In our model this decrease of the monolayer thickness is naturally explained by the splay of the hydrocarbon chains. The relationship between the monolayer thickness z and its initial value z_0 is given by (3). Taking into account that for the H_{II} phase the trace of the tilt tensor $t^\xi_{\ \xi} = \frac{2}{\sqrt{3}}\frac{1}{a}$, the linear dimension of a unit cell is $a \simeq 3\,\mathrm{nm}$ [26], and the initial thickness $z_0 \simeq 1.5\,\mathrm{nm}$, we obtain $\frac{z}{z_0} \simeq 0.75$ in agreement with the result [26].

In spite of reasonable agreement with the experimental data, the suggested model is, definitely, an approximation illustrating the effects of tilt rather than pretending to complete description of the structure and energetics of the inverted mesophases. Indeed, we excluded from consideration the two other possible deformations, namely, the monolayer bending and area stretching. Accounting for these deformations besides the tilt requires minimization of the overall energy within the geometrical constraints and the related determination of the new distributions of tilt, molecular stretching and curvature along the dividing surface. Realization of this program is complicated and goes beyond the goal of the present work. However it is obvious, that the extended model will allow for relaxation of the energy and for a better determination of the tilt modulus κ_θ, which is overestimated in (18).

The further development of the model is also required by the experimental results. Indeed, in our picture the fragments of monolayers constituting a unit cell of an inverted mesophase remain flat and, thus, form the angles along their lines of intersection. Although within the framework of our model such sharp intersections do not result in any singularities of the energy and are in accord with equilibrium between the contacting cassettes, in reality the angles are smoothen out, as it is seen on the reconstructed profiles of the electron density [24]. The most probable reason for this smoothening is the steric repulsion between the polar groups of amphiphilic molecules along the lines of intersection, which is not taken into account by the model. The resulting bending of the monolayer and the related changes in the tilt distribution have to be considered by the more sophisticated approach.

We are grateful to Richard Epand, Sol Gruner, Wolfgang Helfrich, Sergey Leikin, Adrian Parsegian, David Siegel and Richard Templer for fruitful discussions.

References

1. V. Luzzati, in *Biological membranes*, edited by D. Chapman, (Academic Press, 1968), Vol. 1, pp.71-123.
2. J.M. Seddon, N. Zeb, R.H. Templer, R.N. McElhaney, D.A. Mannock, Langmuir **12**, 5250 (1996).
3. M.A. Spivak, *Comprehensive Introduction to Differential Geometry* (Perish. Wilmington, DE, 1979).
4. B. Pansu, E. Dubois-Violette, Coll. Phys. **C7**, 281 (1990)
5. S.A. Safran, L.A. Turkevich, P. Pincus, J. Phys. France **45**, L-69 (1984).
6. M.M. Kozlov, V.S. Markin, Biofizika **28**, 255 (1983).
7. D.P. Siegel, R.M. Epand, Biophys. J. **73**, 3089 (1997).
8. D.P. Siegel, Biophys. J. **65**, 2124 (1993).
9. J.M. Seddon, Biochim. Biophys. Acta **1031**, 1 (1990).
10. W. Helfrich, Z. Naturforsch. **28 c**, 693 (1973).
11. S.M. Gruner, Proc. Natl. Acad. Sci. USA **82**, 3665 (1985).
12. A. Ben-Shaul, in *Handbook of Biological Physics*, edited by R. Lipowsky, E. Sackmann (Elsevier Science BV, Amsterdam, 1995), p. 359.
13. J.N. Israelachvili, *Intermolecular and surface forces*, 2nd ed. (Academic Press Inc., London, LTD., 1985)
14. D.A. Anderson, S.M. Gruner, S. Leibler, Proc. Natl. Acad. Sci. USA **85**, 5364 (1988).
15. G.L. Kirk, S.M. Gruner, D.E. Stein, Biochemistry **23**, 1093 (1984).
16. M.W. Tate, S.M. Gruner, Biochemistry **28**, 4245 (1989).
17. P.M. Duesing, R.H. Templer, J.M. Seddon, Langmuir **13**, 351 (1997).
18. S. May, A. Ben-Shaul, Biophys. J. **73**, 2427 (1997).
19. M.M. Kozlov, S. Leikin, R.P. Rand, Biophys. J. **67**, 1603 (1994).
20. M.W Matsen, F.S. Bates, Macromol. **29**, 7641 (1996).
21. M.W. Matsen, M. Schick, Phys. Rev. Lett. **72**, 2660 (1994); S.P. Gido, D.W. Schwark, E.L. Thomas, Macromol. **26**, 2636 (1993).
22. G.H. Fredrickson, E. Helfand, J. Chem. Phys. **87**, 697 (1987).
23. M. Hamm, M.M. Kozlov, (submitted).
24. D.C. Turner, S.M. Gruner, Biochemistry **31**, 1340 (1992).
25. V. Luzzati, R. Vargas, A. Gulik, P. Mariani, J.M. Seddon, E. Rivas, Biochemistry **31**, 279 (1992).
26. R.P. Rand, N.L. Fuller, Biophys. J. **66**, 2127 (1994).
27. J.W. Gibbs, *On the Equilibrium of Heterogeneous Substances. 1876/1878* in: *The Collected Works of J.Willard Gibbs* (New Haven, Yale University Press, 1948), Vol. 1.

28. S. Leikin, M.M. Kozlov, N.L. Fuller, R.P. Rand, Biophys. J. **71**, 2623 (1996).
29. F.C. Frank, Discuss. Faraday. Soc. **25**, 19 (1958).
30. C.-M. Chen, T.C. Lubensky, F.C. MacKintosh, Phys. Rev. E **51**, 504 (1995).
31. S.A. Safran, *Statistical thermodynamics of surfaces, interfaces, and membranes* (Addison-Wesley, 1994).
32. It should be noted, however, that in lattices of more complicated geometry, such as *bcc* or *Fd3m* where a unit cell consists of cassettes of different shapes, the bending contribution to the energy proves to be different from that of *bcc* and *fcc* in spite of the similar topology. The corresponding calculations go beyond the purposes of this study and will be published elsewhere.
33. This reasoning can not be extended straightforwardly to the lattices whose unit cells involve cassettes of different shapes.
34. S. Alexander, J. McTague, Phys. Rev. Lett. **41**, 702 (1978).
35. S. Alexander, J. Phys. France Colloq. **46**, C3-33 (1985).
36. D. Hone, J. Phys. France Colloq. **46**, C3-21 (1985).
37. Our model results in the energy of the *bcc* phase slightly higher than that of the *fcc* phase (the result not shown). This is of interest in the light of discussion of relationship between the *fcc* and *bcc* phases in colloidal crystals [33], [J. Phys. France Colloq. C3, suppl. N3, Vol. 46, 1985] and deserves further analysis we plan to present elsewhere.
38. I. Szleifer, D. Kramer, A. Ben-Shaul, W.M. Gelbart, S.A. Safran, J. Chem. Phys. **92**, 6800 (1990).